Yan *et al. Biochar (2026) 8:54*
https://doi.org/10.1007/s42773-026-00571-6

Biochar

ORIGINAL RESEARCH

Open Access

Influence of (nano-)biochar-based fertilizer on rice plant growth and metal(loid) uptake under the co-exposure of cadmium and arsenic in a life-cycle greenhouse study

Xingyu Yan[1,3], Jing Liu[1,3*], Wenhui Li[1,3], Weiying Feng[2,3], Jiawei Wang[1,2,3], Zhongxiang Cao[1,2,3], Jining Li[3,4*], John P. Giesy[3,5,6,7] and George P. Cobb[3,5]

Abstract

The low fertilizer utilization efficiency and metal(loid) contamination have become dual challenges that constrain the production of rice and thus food security. To address these issues, a life-cycle greenhouse study was conducted with rice (*Oryza sativa*) grown in soil co-contaminated with cadmium (Cd) and arsenic (As) and treated with several synthetic fertilizers. These fertilizers included regular fertilizers (F), biochar-based fertilizers (BF) and nano-biochar-based fertilizers (NBF), each formulated with varying nitrogen:phosphorus:potassium (N:P:K) ratios (I, II, and III). The results revealed a differential suppression of Cd (strongest under F-I, followed by NBF-III) and As (strongest under F-II, followed by NBF-I) in rice grains, attributable to disparities in their environmental chemistry, bioavailability, and plant-mediated uptake and translocation mechanisms. While BF enhanced catalase and alkaline phosphatase activities, NBF more effectively stimulated urease activity throughout the 0–10 cm layer and sucrase activity in the deeper 5–10 cm zone. Notably, NBF increased soil metabolic diversity under Cd and As stress while strengthening the genetic regulatory capacity and environmental adaptability of microbial communities. Furthermore, NBF dynamically regulated the migration of Cd and As into porewater, resulting in more stable and effective immobilization compared to BF and F treatments. These findings highlight that the application of biochar, particularly nano-biochar, for paddy soil remediation necessitates a contaminant-specific and nutrient-managed strategy. Tailoring both the biochar type and the accompanying N:P:K ratio is crucial for targeting the biogeochemical behavior of the dominant contaminant, thereby ensuring grain safety and supporting sustainable rice production.

Highlights

- Nano-biochar-based fertilizers (NBF) promoted rice tillering and heading processes.
- The N:P:K ratio played a significant role in regulating the soil system and Cd and As accumulation in rice.
- NBF boosted soil enzyme activities and regulated microbial composition.
- The mitigation effects of BF and NBF were strongly dependent on the N:P:K ratio.

*Correspondence:
Jing Liu
liu_jing@email.sdu.edu.cn
Jining Li
ljn006@126.com
Full list of author information is available at the end of the article

Keywords Controlled-release fertilizer, Co-contamination, Porewater dynamics, Soil enzymes, Microbial community, N:P:K stoichiometry

Graphic Abstract

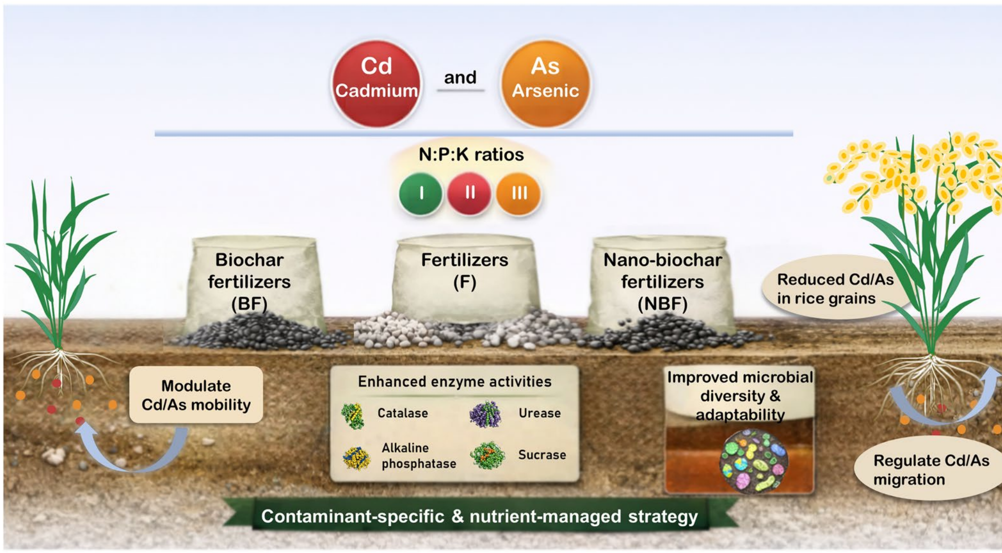

1 Introduction

It is estimated that by 2030, the global population will reach 8.6 billion, placing unprecedented pressure on agricultural systems to increase crop yield and quality (Wang et al. 2022; Raza et al. 2025; Zulfiqar et al. 2024). Historically, this demand has been met largely through extensive fertilizer use, which has boosted yields by approximately 50% (Chen et al. 2018) but with critically low nutrient use efficiency, with reported decreases of 40–70% for nitrogen (N), 80–90% for phosphorus (P), and 50–70% for potassium (K) (Cui et al. 2018; Wu et al. 2018; He et al. 2022; Wang et al. 2022; Liu et al. 2025). Such inefficiency not only wastes resources but also drives soil acidification and mobilization of toxic metal(loid)s, such as cadmium (Cd) and arsenic (As), promoting their accumulation in staple crops like rice (Srivastav et al. 2023). This risk can be further exacerbated by the application of biosolids from wastewater treatment, which introduces additional metal(loid)s inputs into agricultural soils (Hao et al. 2025; Xue et al. 2025). Addressing the dual challenge of low fertilizer efficiency and associated metal(loid) contamination is thus crucial for achieving both food security and nutritional safety. In response, slow-release fertilizers (SRFs) have emerged as a promising strategy to enhance nutrient use efficiency while mitigating environmental triggers of metal(loid) mobilization.

As advanced nutrient delivery systems, SRFs are designed to release nutrients gradually and synchronously with crop demand across growth stages (Lu et al. 2023), and can significantly improve N use efficiency compared with conventional fertilizers (Dong et al. 2019). The incorporation of agricultural waste into SRF formulations further improves their environmental sustainability and economic feasibility (Shi et al. 2020). However, many existing SRFs still suffer from relatively short nutrient release duration, limited nutrient-loading capacity, and a narrow focus on nutrient use efficiency alone (Ji et al. 2024). Much less attention has been paid to additional functionalities, such as mitigating soil metal(loid) contamination and improving soil physicochemical properties during agro-ecosystem restoration. Therefore, there is an urgent need for novel fertilizers that possess controlled nutrient release properties and the ability to remediate metal(loid)-contaminated soils. Biochar emerges as a promising material for such designs.

Biochar is a carbon-rich, porous material usually produced by thermochemical transformation processes at temperatures ranging from 300 to 700 °C (Yuan et al. 2025). It features a large specific surface area, abundant pore structure, diverse surface functional groups, and strong adsorption capacity (Tao et al. 2024; Yuan et al. 2025). Loading nutrients onto biochar has been shown to improve the overall performance of fertilizers in crop production (Faloye et al. 2020). Compared with traditional fertilizers, biochar-based fertilizers (BF) show significant advantages in nutrient retention and slow-release behaviour (Chen et al. 2025). Nano-biochar further amplifies these advantages through its higher reactivity and greater specific surface area (Chausali et al. 2021; He et al. 2022). Nano-biochar-based fertilizers (NBF) have been reported to improve crop yield and quality, compared to conventional fertilizers with equivalent nutrient content (Wang et al. 2018).

Beyond their functionality as nutrient carriers, biochar and nano-biochar can modify soil physicochemical properties and possess significant potential for the remediation of metal(loid)-polluted soils. For instance, biochar/nano-biochar can adjust soil pH and cation exchange capacity (CEC), thereby promoting the nutrient retention (Jin et al. 2024), improving soil structure, and providing suitable habitats for microorganisms that shape microbial community composition and stimulate key enzyme activities (e.g., urease, invertase, dehydrogenase and alkaline phosphatase) (Gai et al. 2024; Liu et al. 2024). Their active functional groups and porous structure can also facilitate immobilization of potentially toxic metal(loid)s like Cd and As, thereby decreasing their bioavailability and accumulation in crops (Liu et al. 2024). However, the suitability of BF/NBF for a specific soil type remains unclear; likewise, their efficacy in mitigating metal(loid) contamination has yet to be evaluated (Sani et al. 2023).

This study systematically explored the effects of BF/NBF on soil properties and rice growth performance under combined Cd and As stress. Specifically, we aimed to: (1) clarify the regulatory effect of BF/NBF on key microbial communities and soil enzyme activities; (2) investigate the capacity of BF/NBF to remediate the migration and bioavailability of Cd and As; and (3) reveal their contribution to alleviating metal(loid) stress in rice and improving rice yield and quality. By integrating nutrient management with in situ remediation, this study seeks to enhance fertilizer nutrient utilization while advancing practical strategies for remediation of polluted farmland, thereby contributing to sustainable agricultural production.

2 Materials and methods

2.1 Materials and chemicals

Biochar was produced from rice straw. Commercial fertilizer (15-15-15) was purchased from Hebei Dewoduo Biotechnology Co., Ltd., China. All chemical reagents were of analytical grade and procured from commercial suppliers. Standard reference materials GBW07386(GSS-30), GBW10010a(GSB-1a) and BW10015a(GSB-6a) respectively for plant, rice and soil sample digestion validation were purchased from Beijing Century Aoke Biotechnology Co., Ltd. and used to evaluate metal contents. The mixed standard solution of 27 elements for water sample digestion validation was purchased from the Henan Standard Reference Material Research and Development Center.

2.2 Synthesis and characterization of fertilizers

2.2.1 Preparation and characterization of biochar and nano-biochar

Rice straw was washed with ultrapure water, oven-dried at 70 °C for 24 h, cut into 2 cm segments, and ground into fine powder with a grinding machine (AQ-180E, Cixi Naiou Electrical Appliance Co., Ltd.). The powder was then pyrolyzed in a tube furnace (TF55035C-1, Thermo) at 500 °C for 2 h to produce biochar with high carbon stability, a well-developed pore structure and preserved functional groups (Lu et al. 2023). The obtained biochar was subsequently milled into nano-biochar using a high-throughput ball mill (MB-24S, Zhejiang Meibi Instrument Co., Ltd.). The milling process was conducted in a 15 mL steel tube containing mixed grinding media (five 6 mm and four 5 mm steel balls) at 50 Hz for 15 min, with a 30 s pause after each 1 min run. The pH and electrical conductivity (EC) of biochar (biochar: water = 1:2.5, w/v) were determined using a DZB-712 portable multi-parameter analyzer (Shanghai Leici Scientific Instrument Factory). The surface morphology of biochar and nano-biochar was characterized with a scanning electron microscopy (SEM, Quanta 250 FEG, FEI) (Figure S1). The SEM revealed abundant nano-sized (< 100 nm) particles in the ground biochar powder, supporting its classification as nano-biochar. Dynamic light scattering (DLS; Brookhaven BI-200SM) of ethanol-dispersed samples (20 mgL^{-1}, after 30 min ice-bath sonication) yielded a hydrodynamic diameter of 764.8 ± 127.3 nm, suggesting particle aggregation in suspension, a typical characteristic of nano-biochar dispersions.

2.2.2 Synthesis of biochar-based and nano-biochar-based fertilizers

Biochar based fertilizers (BF) or nano-biochar-based fertilizers (NBF) were prepared using urea ($CO(NH_2)_2$), ammonium dihydrogen phosphate ($NH_4H_2PO_4$), and potassium chloride (KCl) as the core fertilizers (64%), rice straw biochar or nano-biochar as the auxiliary material (16%) and sodium-based bentonite as the binding agent (20%). The 64:16 ratio of core fertilizers to biochar/nano-biochar was selected as an optimal balance between nutrient supply and functional enhancement, as demonstrated in previous research (Lu et al. 2023). Three

N:P:K ratios were prepared as I (15:15:15), II (50:9:25), and III (55:7:25), respectively, corresponding to prevalent commercial products. Nine fertilizer formulations were systematically prepared by combining three N:P:K ratios with three matrix types (unmodified control [F], biochar-modified [BF], and nano-biochar reinforced [NBF]). For granulation, all raw materials for each formulation were loaded into a rotating disc granulator (32 rpm, 45° inclination). During rotating, the mixture was sprayed with water (15 mL per 100 g of raw materials) for homogenization and agglomerated into spherical granules. The resulting granules were sieved through 2 mm and 5 mm meshes to remove oversized and undersized fractions, and the retained product was then dried in a forced-air oven at 40 °C to constant mass.

2.2.3 Physicochemical characterization of fertilizers

Fertilizer particle size was determined by measuring ten randomly selected granules from each treatment with a vernier caliper. Compressive strength was evaluated using a hand-pressing pressure gauge (Dongguan Qilian Electronic Equipment Co., LTD., NK-10). The Brunauer–Emmett–Teller (BET) specific surface area and pore structure were determined by N_2 physisorption at 77 K using a micropore and physisorption analyzer (ASAP2460). Surface morphology and elemental composition of the biochar-based fertilizer were analyzed by SEM–EDS (Quanta 250 FEG, US). Functional groups were identified by Fourier- transform infrared spectroscopy (FTIR) (Vertex 70v, Bruker). The pH and EC were measured in a 1:10 (w/v) fertilizer-water suspension in ultrapure water (18.2 MΩ·cm) (Villada et al. 2024). Ash content was determined as the residue remaining after heating at 700 °C in the tube furnace (Villada et al. 2024).

2.3 Life-cycle experiment of rice plants in a greenhouse

Typical paddy soil was collected from Rizhao, Shandong Province, China. The soil was classified as sandy loam, with a pH of 6.36, organic matter (OM) content of 25.93 g kg^{-1}, hydrolysable N of 122 mg kg^{-1}, available P of 39.8 mg kg^{-1}, available K of 128 mg kg^{-1}, Cd content of 0.08 mg kg^{-1}, and As content of 5.08 mg kg^{-1}. After air-drying, the soil was ground to pass a 2 mm sieve. The concentrations of Cd and As in the soil were adjusted to 0.4 mg kg^{-1} and 15 mg kg^{-1}, which are approximately half of the threshold risk values in farming soils by many regulatory organizations. Although such concentrations are generally considered safe for crop cultivation, studies have reported that they can still induced toxic effects.

Nine treatment groups were established: (1) control fertilizer treatments (F-I, F-II, F-III); (2) biochar-based fertilizer treatments (BF-I, BF-II, BF-III) and (3) nano-biochar-based fertilizer treatments (NBF-I, NBF-II, NBF-III). Fertilizers were applied at an equivalent field rate of 600 kg ha^{-1} and incorporated 3–5 cm below the soil surface in pots (3 L volume, 180 mm height) containing 2.5 kg of treated soil. Each treatment included five replicate pots. Two uniform 2-week-old rice seedlings (*Oryza sativa*), cultivated under controlled conditions in the incubator, were transplanted into each pot. Pots were treated as independent experimental units, and within-pot variation between seedlings was not considered in the statistical analysis. To minimize spatial heterogeneity in the greenhouse environment, pots were re-positioned every two weeks following a systematic rotation pattern in which all rows were shifted in one direction and all columns in the perpendicular direction. Water management and disease control followed field practice (Text S1).

Rice plants were manually harvested after 108 d of cultivation in the greenhouse. Spikes were dried, threshed, and weighed. A portion of the soil samples was stored at −80 °C for 16S rRNA analysis of soil microbial communities (Text S2). Another portion was air-dried at 40 °C for physicochemical analysis (Text S3). The remaining portion was kept at 4 °C for soil enzyme assay following protocols provided by the manufacturer (Grace Biotechnology, China). Amylose and protein content in rice were determined using a grain analyzer with an embedded reference standard for calibration (SupNIR-1251, Beijing Titan Instruments Co., Ltd, China). The digestion procedure for rice, soil samples and their reference standards as quality control was adapted from USEPA Method 3050B40 (EPA 1996). Concentrations of Cd and As in the digestates were determined by an inductively coupled plasma mass spectrometer (ICP-MS, Agilent 7800, USA) (Text S4).

2.4 Statistical analyses

Differences among treatments were assessed using generalized linear models (GLM) with biochar treatment (F, BF, NBF) and N:P:K ratio (I, II, III) as fixed factors. The biochar × N:P:K interaction was evaluated using post hoc ANOVA on the fitted GLMs. When a significant interaction was detected ($p < 0.05$), we conducted simple-effects (conditional) comparisons: (i) differences among biochar treatments within the same N:P:K ratio, and (ii) differences among N:P:K ratios within the same biochar treatment. Results were presented as mean ± standard error (SE) and differences were considered significant at $p < 0.05$. With the 3 × 3 factorial design and 5 replicates per treatment (total N = 45), a post-hoc power analysis was conducted and indicated ~ 65% power to detect medium effect sizes (f = 0.25) and ~ 95% power to detect large effects at α = 0.05, which are of primary interest in this preliminary investigation. All analyses were conducted in R (R 4.3.1), and figures were prepared in R and Adobe Illustrator (2024).

3 Results and discussion

3.1 Characterization of biochar-based fertilizers

3.1.1 Physicochemical properties of fertilizers

The physicochemical properties of the fertilizers are presented in Table 1. Notably, biochar and nano-biochar increased the BET specific surface area and porosity. Among all formulations, NBF-II exhibited the highest surface area of 2.04 $m^2\ g^{-1}$, exceeding that of all the other fertilizers. This demonstrates that nano-carbonization can further refine pore structure and enhance nutrient retention capacity (Zhao et al. 2023). Compressive strength is a critical determinant of fertilizer performance, as it governs water penetration and nutrient release behaviour. Compared to F groups, BF and NBF had decreased compressive strength, likely due to the filling and dispersion effects of biochar/nano-biochar, which increased internal porosity while maintaining sufficient mechanical integrity, which is key for sustained nutrient release under field conditions. Compared with F, BF and NBF slightly increased the pH and significantly lowered EC of fertilizer-water suspension. This suggests that nano-biochar formulations can help mitigate soil acidification and salinity stress, thereby optimizing rhizosphere conditions for plant growth (Bolan et al 2023). Moreover, the higher ash content of BF and NBF reflects increased inorganic inputs from the biochar and nano-biochar components, which can benefit soil fertilization by providing a slow-release nutrient source.

3.1.2 Surface morphology of fertilizers

SEM revealed distinct treatment-dependent differences in particle morphology and porous structure among the fertilizer formulations (Fig. 1a). The corresponding EDS spectra (Fig. S2–S4) demonstrated the expected elemental signals of carbon (C), N, oxygen (O), sodium (Na), P, silicon (Si), and K, with variations in peak intensity and spatial distribution across treatments. In F treatments, particles were relatively compact and the signals were dominated by nutrient-related elements (e.g., N, P, K), consistent with dense granules. In contrast, BF and NBF exhibited a distinct biochar-derived carbonaceous matrix with a more developed porous texture. Their EDS spectra showed enhanced C signals along with enhanced K, Si, and P, suggesting the coexistence of a porous carbon framework and nutrient-bearing phases. This microstructure is consistent with the partial preservation of plant vascular bundle architecture during straw carbonization, forming a honeycomb-like carbon network (Gu et al. 2023). Such porosity can increase specific surface area and provide diffusion pathways that favor solute adsorption/retention and controlled nutrient release.

While SEM highlights structural contrasts, FTIR primarily reports major functional groups in the bulk composite (Fig. 1b). BF/NBF and F share broadly similar band positions, with differences mainly reflected in relative intensity and band broadening rather than the emergence of many new peaks. The broad band near ~ 3400 cm^{-1} corresponds to overlapping O–H and N–H stretching vibrations, which can arise from –OH groups on biochar surfaces and N–H vibrations from urea-derived species (Liu et al. 2020b; Xiang et al. 2021). The presence of two N sources ($CO(NH_2)_2$ and $NH_4H_2PO_4$) does not necessarily produce multiple resolved "amine/amino" bands in solid-state FTIR spectrum, because $NH_4H_2PO_4$ contribute mainly to

Table 1 Physicochemical properties of the fertilizers

Treatment	Surface area ($m^2\ g^{-1}$)	Compressive strength (N)	pH	EC(ms cm^{-1})	Ash content (%)
F-I	0.7302	10.20 ± 0.89Aa	7.71 ± 0.05Aa	65.70 ± 1.40Ab	–
BF-I	1.8752	9.35 ± 1.16Aa	7.92 ± 0.08Aa	52.55 ± 5.75Aa	33.38Aa
NBF-I	1.0084	6.20 ± 0.35Ab	7.64 ± 0.22Aa	31.05 ± 0.55Ac	33.66Aa
F-II	0.9509	4.82 ± 0.63Ba	5.43 ± 0.06Bb	32.65 ± 0.35Ba	44.76Ab
BF-II	0.9187	4.24 ± 0.49Ba	6.00 ± 0.00Ba	28.10 ± 0.10Bab	52.2Ba
NBF-II	2.0411	4.71 ± 0.47Aa	5.94 ± 0.01Ba	27.80 ± 0.00Bb	52.63Ba
F-III	0.7871	5.87 ± 0.32Ba	5.42 ± 0.04Ba	34.20 ± 0.00Bb	42.69Ab
BF-III	1.2558	4.54 ± 0.16Ba	5.60 ± 0.01Cab	27.60 ± 0.10Ca	58.99Ba
NBF-III	1.8171	4.73 ± 0.24Aa	5.81 ± 0.05Bb	29.60 ± 0.40Bab	54.48Ba

Note: I, II, and III represent three different N:P:K ratios. F represents the fertilizer without biochar/nabo-biochar, BF denotes biochar-based fertilizers, and NBF indicates nano-biochar-based fertilizers. Uppercase letters indicate the differences between N:P:K ratios within the same fertilizer type ($p < 0.05$). Lowercase letters indicate differences between treatments with the same N:P:K ratio ($p < 0.05$). Data are reported as the mean ± SE (N = 5)

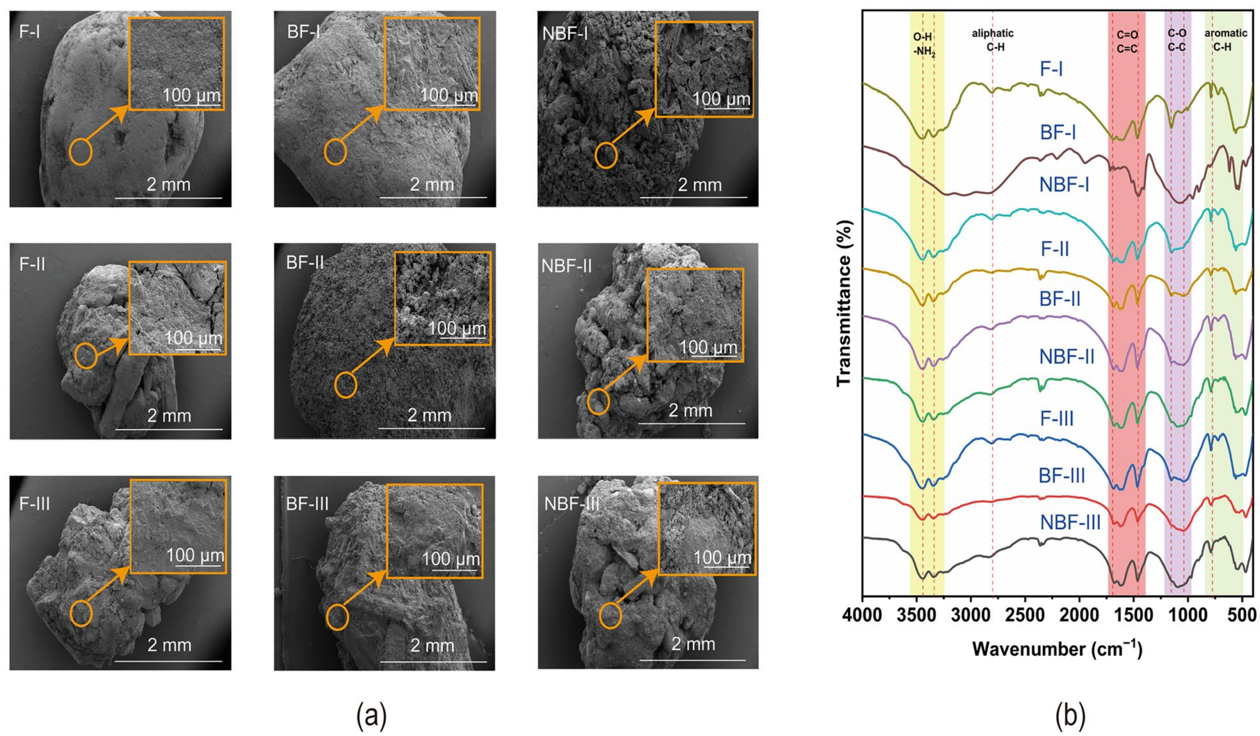

Fig. 1 Morphological and chemical characterization of fertilizer formulations using **a** SEM and **b** FTIR spectra of the corresponding formulations

phosphate vibrations and its N–H features often overlap with the O–H envelope. Bands at 2800–2950 cm^{-1} correspond to aliphatic C–H stretching, and features in the 1500–1600 cm^{-1} reflect aromatic C=C and C=O related vibrations (Cheng et al. 2022). C-related bands are expected even in the F group because urea contains a C=O group and formulation additives/coatings may also contribute additional organic signatures. Thus, C/O-related bands should not be taken as exclusive indicators of biochar presence, but rather as signals from the composite's organic and inorganic constituents (Dong et al. 2019). Peaks around 518–661 cm^{-1} are consistent with Si–O–Al vibrations from bentonite, supporting its role as a mineral binder in the granules. The 1000–1100 cm^{-1} region contains overlapping signals from C–O (alcohol), Si–O (bentonite) and the P–O (phosphates) vibrations, while the band near 1159 cm^{-1} is attributable to the phosphate-related P–O bond vibrations (Nayak et al. 2024; Das and Satapathy 2024). These FTIR features, together with SEM/EDS, support a composite structure in which bentonite provides a silicate framework and binding phase, while biochar/nano-biochar contributes an aromatic C matrix and O-containing surface functionalities. The interaction between bentonite and the carbonaceous phase is likely governed by (i) physical encapsulation/bridging that enhances granule integrity, (ii) H-bonding between mineral surface –OH groups and biochar O-containing moieties, and (iii) electrostatic interactions and cation exchange involving nutrient ions (e.g., NH_4^+ and K^+).

Overall, the combined SEM, EDS, and FTIR evidence indicates that BF/NBF differ most strongly from F in microstructure (porosity, coating and element distribution), while FTIR confirms the coexistence of biochar-related functionalities and nutrient/mineral phases, without implying the formation of numerous distinct N-functional groups on the solid surface. These structural and chemical features indicate that BF and NBF can provide multiple interaction pathways for metal(loid) retention, thereby potentially reducing Cd and As mobility. Meanwhile, the preserved aromatic structures confer mechanical stability and persistence, supporting durable granule structure and longer-term C sequestration (Xu et al. 2022). This combination of reactive surface and structural stability underscores the advantages of (nano-)biochar-based fertilizer systems for sustainable agriculture.

3.2 Soil biological responses to fertilizer treatments

3.2.1 Responses of soil enzymes

Soil enzymes are highly sensitive to exogenous inputs and serve as reliable indicators of microbial activity, nutrient cycling capacity, and environmental stress (Yang et al. 2016). This study examined four key enzymes: sucrase

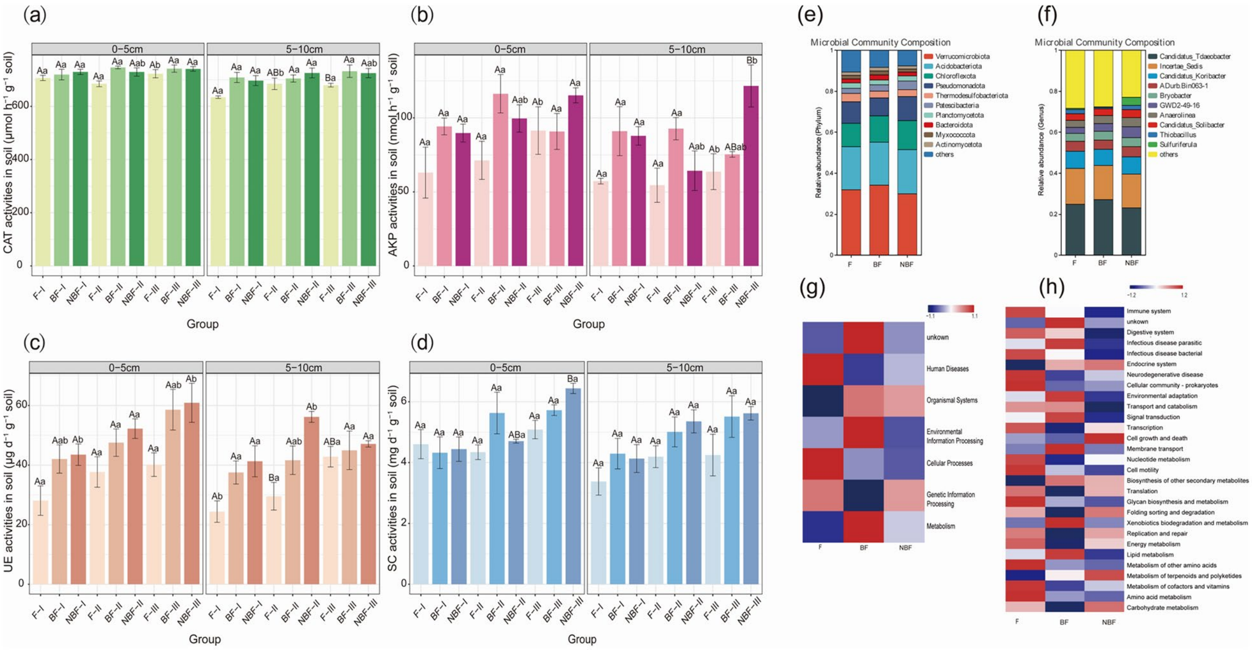

Fig. 2 Soil biological responses to different fertilizer treatments. **a**–**d** Soil enzyme activities at two soil depths (0–5 and 5–10 cm): **a** catalase (CAT), **b** alkaline phosphatase (AKP), **c** urease (UE), and **d** sucrase (SC). Different letters indicate significant differences based on interaction-aware post hoc tests ($p < 0.05$) in this factorial design (biochar type × N:P:K ratio). Uppercase letters denote differences among biochar treatments within the same N:P:K ratio at the same depth, while lowercase letters denote differences among N:P:K ratios within the same biochar treatment at the same depth ($p < 0.05$). Data are reported as the mean ± SE (N = 3). **e**–**h** Soil microbial community composition at the **e** phylum and **f** genus levels, and KEGG functional predictions at **g** level 1 and (h) level 2 under different fertilizer treatments.

(SC), urease (UE), alkaline phosphatase (AKP), and catalase (CAT). These four enzymes collectively participate in the biogeochemical cycling of C, N, P, and sulfur (S), respectively. Because the experiment followed a factorial design (biochar type × N:P:K ratio), treatment effects were evaluated using conditional comparisons when interactions were present (Fig. 2).

Across fertilizer types, NPK-II and NPK-III treatments consistently enhanced CAT, AKP, UE, and SC activities compared to NPK-I. Particularly in the 5–10 cm soil layer, F treatments exhibited higher CAT and UE activities, while NBF showed superior SC performance ($p < 0.05$). These results suggest that under equivalent nutritional rates, optimized nutrient compositions (NPK-II and NPK-III) improve microbial conditions and enhance soil enzyme function. Enzyme activities in the soil also differed significantly by biochar type in the fertilizer ($p < 0.05$). BF generally promoted greater CAT and AKP activities, whereas NBF more effectively stimulated UE activity throughout the 0–10 cm profile and SC activity in the deeper 5–10 cm layer ($p < 0.05$). Depth-specific patterns were evident: the 0–5 cm layer showed greater responses to biochar amendments, which was likely due to higher OM content and microbial abundance near the surface. Within this 0–5 cm layer, CAT activity in BF-II and NBF-II treatments exceeded that of F-II ($p < 0.05$). In the 5–10 cm layer, BF-III and NBF-III also outperformed F-III ($p < 0.05$). A similar trend was observed for AKP, with BF-III and NBF-III showing clear enhancement over F-III in the 5–10 cm layer ($p < 0.05$), and both BF-II and NBF-II exhibiting significantly higher AKP activity than F-II in both layers ($p < 0.05$). UE enzyme displayed strong activation in the NBF treatment. In the 0–5 cm layer, NBF-I and NBF-III showed greater UE activity than the corresponding F groups. This pattern persisted in the 5–10 cm layer, where the BF-I, NBF-1 and NBF-II treatments exceeded F in UE activity ($p < 0.05$). SC activity also increased under NBF compared to BF and F, indicating nano-biochar's greater capacity to promote C-cycling processes. These enhancing effects can be attributed to multiple mechanisms by which biochar improves microbial functioning. Biochar supplies labile C and N that serve as substrates for microbial metabolism, stimulating extracellular enzyme production. It also enhances the bioavailability of soluble OM in soil, thereby increasing the activity of C-cycling enzymes such as SC (Zhang et al. 2024). Compared to traditional biochar, nano-biochar provides a higher specific surface area and more microsites for microbial colonization, further enhancing microbial activity (Shahzadi et al. 2025). Enzyme activities were generally higher near the surface, which indicates that the enzymatic sensitivity is closely related to the fertilizer placement depth (3–5 cm). Compared with conventional biochar, nano-biochar exhibited stronger migration ability and soil structure modification capacity, though its migration efficiency declined with depth (Li et al. 2024). Overall, NBF reduced the contrast between surface and subsurface layers, indicating a more balanced and persistent regulatory effect on soil enzymatic systems. By facilitating the downward transport of functional substances and extending microbial activity into deeper soil layers, NBF supports a more vertically distributed and resilient soil biochemical environment.

3.2.2 Shifts in soil microbial community structure

The α diversity indices (chao1, Shannon, Simpson, ACE) and β diversity analyses indicated no differences in bacterial richness or diversity among the F, BF, and NBF treatments ($p > 0.05$). Nevertheless, community composition differed among treatments. The 10 predominant bacterial phyla included Verrucomicrobiota, Acidobacteriota, Chloroflexota, Pseudomonadota, Thermodesulfobacteriota, Patescibacteria, Planctomycetota, Bacteroidota, Myxococcota, and Actinomycetota (Fig. 2a). Verrucomicrobiota dominated in all groups (about 30%) but was slightly more abundant in F, indicating that biochar addition may modestly suppress its proliferation. Acidobacteriota (approximately 20–25%), a sub-dominant phylum associated with decomposition of refractory organic carbon and with metal(loid) fixation, was more abundant in NBF, aligning with its known ability to alleviate As-induced stress (Cao et al. 2024). Chloroflexota abundance increased in BF and NBF (about 20%), indicating improved soil nutrient availability under biochar amendments. NBF also increased the abundance of Proteobacteria, Acidobacteria, and Chloroflexi, which reduced the availability of Cd in the soil through complexation and adsorption capacity (Zhang et al. 2022). Pseudomonadota were more abundant in NBF than in F and BF, revealing that NBF created a soil environment more favorable for their proliferation. Although less abundant, Actinomycetota and Bacteroidota play significant roles in OM decomposition and N and P metabolism (Zhang et al. 2022). Overall, BF and NBF, especially NBF due to its large specific surface area and intricate porous structure, provided microhabitats for microorganisms and simultaneously altered the physicochemical properties of soil, thereby leading to shits in community composition. BF and NBF also created a sheltered environment for microorganisms against microarthropod predation and supplied additional nutrients that supported microbial growth (Wang et al. 2025). Furthermore, the observed shifts in genus-level composition were closely aligned with BF and NBF-induced increases in soil pH (Fig. 2b).

KEGG functional predictions showed broadly similar functional profiles among treatments (Fig. 2c). Metabolism dominated (~80%), followed by genetic information processing (~10%). Cellular processes, environmental information processing, and organismal system functions each contributed 2%–5%, while human-disease-related pathways accounted for < 2%. These results highlight that bacterial communities primarily support material cycling and transformation, thereby promoting plant growth (Yan et al. 2022). The 29 KEGG level-2 pathways were further quantified (Fig. 2d). Core functions included carbohydrate, amino acid, lipid, and energy metabolism, which indicates that soil microbial communities across all treatments maintained essential metabolic functions for nutrient turnover. However, functional distribution varied by treatment. Group F showed lower metabolic activity but stronger enrichment in pathways related to cellular processes and human-diseases analogues, suggesting increased investment in stress responses. The BF treatments enhanced metabolic and environmental information pathways, including secondary metabolite biosynthesis, membrane transport, xenobiotic degradation, environmental adaptation, lipid metabolism, infectious disease-related pathways, signal transduction, and catabolism. These observations indicate that BF provided an additional C source and a modified microenvironment. Compared to F and BF, NBF showed greater abundances in genetic information processing and organismal systems, with notable enhancements in endocrine regulation, terpenoid and polyketide biosynthesis, cell growth and death, protein folding/sorting/degradation, and carbohydrate metabolism. These results indicate that NBF consistently enhanced metabolic diversity, promoted microbial community reconstruction, and enhanced ecological resilience under Cd and As stress.

3.3 Rice growth performance and metal(loid) uptake

3.3.1 Rice plant growth and grain quality assessment

Previous studies have shown that the alkalinity of biochar can reduce soil acidity by releasing cations into the soil (Jin et al. 2024). Similarly, BF can effectively alter the soil chemical environment and improve pH, EC, and CEC (López et al. 2025). Consistent with these findings, the present study showed that BF and NBF helped alleviate soil acidic stress and enhanced reducing conditions, thereby facilitating immobilization of metal(loid)s. Soil pH dropped sharply at the booting stage and increased to a maximum at the heading stage, whereas E_h peaked at booting stage and subsequently decreased, demonstrating the alternation between reductive and oxidative conditions during rice growth (Fig. S5). Compared with

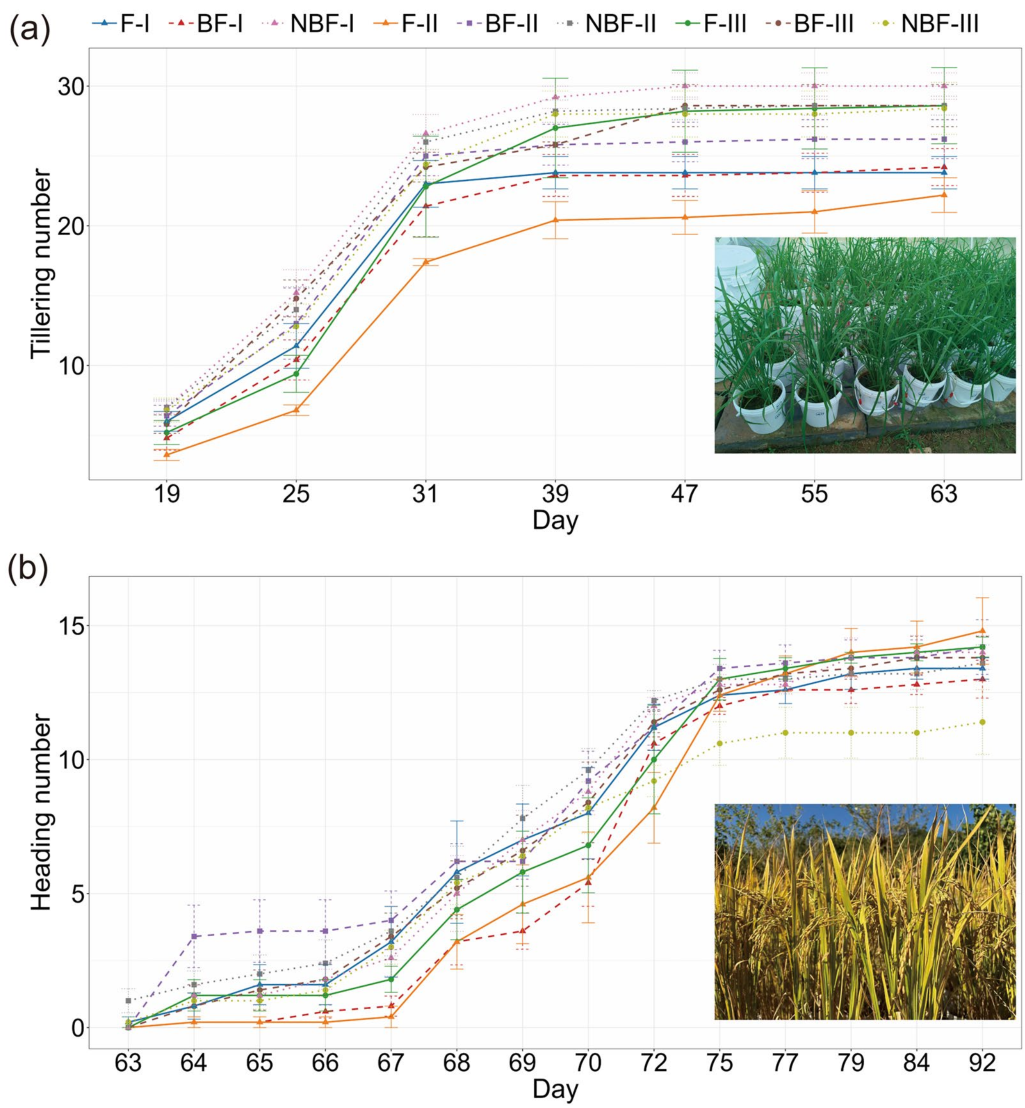

Fig. 3 Temporal dynamics of **a** tillering number and **b** heading number over the full life-cycle of rice under different fertilizer treatments. Data are reported as the mean ± SE (N = 5)

F, both B and NB increased soil pH and decreased E_h during the later growth stages (heading and maturing).

Tillering is a vegetative propagation strategy of grasses in which the main shoot produces lateral shoots called “tillers”. After tillering, rice plants enter the heading stage, during which panicles emerge from the flag-leaf sheath (Fig. 3). NBF markedly boosted tiller formation in the early period and maintained relatively high tiller numbers (Fig. 3a). For example, NBF-I produced more tillers than F-I and BF-I from days 19–25; NBF-II exceeded F-II and BF-II from days 19–55, and NBF-III exceeded F-III and BF-III from days 25–39 ($p < 0.05$). These trends suggest that NBF could continuously release nutrients during the early stage and stimulate tiller production. BF also demonstrated strong regulatory effects, especially in maintaining relatively high tiller numbers during the mid-late tillering stages. In contrast, F consistently showed the lowest tiller counts, indicating lower utilization efficiency of fertilizers. At the onset of heading (Fig. 3b), BF-II treatment initially showed the highest heading rate during the first week. Subsequently, the NBF-II surpassed BF-II and maintained a relatively high heading rate thereafter. During the later stage of heading (days 75–92), the number of heads converged across all treatment groups. These patterns indicate that NBF primarily enhances early development by promoting heading and increasing the early heading rate, whereas final yield did not differ markedly among treatments.

Table 2 Effects of fertilizer treatments on rice yield components

Treatment	Number of effective panicles per plant	Grain number per panicle	100-grain weight (mg)	Yield per pot (g)
F-I	13.80 ± 0.86Aa	88.80 ± 5.94Aa	1604.45 ± 16.73Aa	24.38 ± 0.94Aa
BF-I	12.40 ± 0.51Aa	79.70 ± 4.66Aa	1670.25 ± 21.50Aa	21.51 ± 1.06Aa
NBF-I	13.40 ± 0.68Aa	78.90 ± 4.34Aa	1631.98 ± 19.99Aa	25.87 ± 0.75Aa
F-II	14.00 ± 0.45Aa	91.20 ± 4.63Aa	1674.82 ± 44.27Aa	25.07 ± 0.94Aa
BF-II	14.00 ± 1.05Aa	87.60 ± 4.32Aa	1615.33 ± 20.57Aa	27.36 ± 2.18Ba
NBF-II	13.00 ± 0.55Aa	80.60 ± 7.90ABa	1659.83 ± 23.64Aa	25.27 ± 0.71Aa
F-III	13.00 ± 0.77Aa	88.40 ± 6.97Aa	1619.20 ± 52.18Aa	23.66 ± 2.47Aa
BF-III	13.00 ± 0.32Aa	82.40 ± 4.06Aa	1636.99 ± 29.43Aa	24.87 ± 0.67ABa
NBF-III	10.40 ± 0.81Bb	100.20 ± 5.37Ba	1689.96 ± 20.13Aa	22.18 ± 2.23Aa

Note: Capital letters indicate differences among N:P:K ratios within the same fertilizer type ($p < 0.05$). Lowercase letters indicate differences in the same N:P:K ratio among different fertilizers ($p < 0.05$). Data are reported as the mean ± SE (N = 5)

At harvest, the number of effective panicles per plant in NBF, particularly NBF-III, was lower than that in F and BF ($p < 0.05$) (Table 2). However, the grain number per panicle in NBF-III was significantly higher than in the other treatments ($p < 0.05$). The 100-grain weight in NBF-III also tended to be higher, although this difference was not statistically significant. Since the rice yield mainly depends on the number of effective panicles (Si et al. 2018), eventually, BF-II acheived the highest yield among all treatments ($p < 0.05$). These results suggest that, in addition to biochar type, the N:P:K ratio strongly influences yield outcomes. From a long-term perspective, biochar application generally increases rice yields (Lv et al. 2021), especially in acidic soils (Jeffery et al. 2011), but may exert negative effects on plant growth under calcareous or high-pH conditions (Liang et al. 2014). Therefore, the yield responses to biochar reflect multiple interacting factors, including regional geology, crop type and application conditions. Field experiments further demonstrate that the relationships among crop yields, soil properties, biochar, and climate vary across regions (Laird et al. 2017).

At comparable moisture content, rice grains typically comprise 80–85% starch and 4–10% protein, with starch mainly consisting of amylose and amylopectin (Li et al. 2022). Our study demonstrates that protein content, amylose content, and taste value of rice responded differently to BF and NBF across three N:P:K ratios (Table 2). At NPK-II, both BF and NBF generally reduced protein content, slightly increased amylose content, and improved taste value relative to F, whereas distinct response patterns were observed at NPK-I and NPK-III. In general, greater amylose content is associated with firmer, less sticky cooked rice (Liu et al. 2020a). Moderate reductions in amylose content can improve starch gelatinization during cooking, promote the formation of weak gel networks, and reduce hardness while increasing its viscosity (Tao et al. 2019; Li et al. 2023). Protein exerts an additional, often negative, influence on eating quality: excess protein content can reduce the solubility of starch in hot water and restrict the swelling and

Table 3 Effects of fertilizer treatments on the contents of water, protein and amylose, and taste value of rice

Treatment	Water content (%)	Protein content (%)	Amylose content (%)	Taste value
F-I	9.68 ± 0.14	8.47 ± 0.20Ab	15.32 ± 0.27	75.42 ± 1.07
BF-I	10.46 ± 0.16	10.44 ± 0.22Aa	14.40 ± 0.27	71.74 ± 1.16
NBF-I	9.88 ± 0.10	8.43 ± 0.27Ab	15.37 ± 0.24	75.82 ± 1.12
F-II	10.12 ± 0.28	9.87 ± 0.10Ba	14.62 ± 0.27	71.18 ± 0.77
BF-II	10.58 ± 0.07	9.21 ± 0.08Bab	14.89 ± 0.81	73.77 ± 2.28
NBF-II	9.75 ± 0.04	8.77 ± 0.12Ab	15.11 ± 0.05	74.66 ± 0.04
F-III	9.74 ± 0.26	9.96 ± 0.36Bb	14.76 ± 0.25	72.31 ± 1.24
BF-III	10.36 ± 0.23	8.97 ± 0.05Ba	15.31 ± 0.05	75.64 ± 1.04
NBF-III	10.03 ± 0.06	10.10 ± 0.10Bb	15.34 ± 0.22	73.80 ± 0.90

Note: Capital letters indicate the differences among different N:P:K ratios within the same fertilizer type ($p < 0.05$). Lowercase letters indicate differences in the same N:P:K ratio among different fertilizers ($p < 0.05$). Data are reported as the mean ± SE (N = 5) leaching, thereby making cooked rice harder and less viscous (Li et al. 2022). Thus, an appropriate balance—relatively lower protein content combined with suitable amylose levels—tends to favor better palatability. The BF and NBF treatments, particularly under NPK-II, helped shift this balance toward improved the sensory quality of rice grains (Table 3).

3.3.2 Mitigation of Cd and As mobility in the soil-rice system

The concentrations of Cd and As in porewater exhibited pronounced temporal fluctuations during rice growth, which significantly influenced their accumulation in rice tissues (Figs. 4 and 5). Across all treatments, the concentration of Cd in porewater generally decreased during the seedling stage, followed by a sharp peak at tillering stage, and decreased again toward maturity (Fig. 4a). In contrast, concentrations of As in porewater increased during seedling, decreased during tillering, briefly rebounded at heading, and declined again toward maturity (Fig. 4b). Because grain filling and final allocation of Cd and As to edible tissues occur mainly from heading to maturity (Liu et al. 2019), the maturation stage is a critical window that ultimately determines metal(loid) accumulation in rice grain. Thus, the lower porewater concentrations observed at maturity under several BF and NBF treatments are especially relevant for food safety.

These stage-dependent patterns can be explained by shifts in soil redox conditions driven by flooding, root O_2 release, and intermittent water loss. Temporary increases in Cd and As around day 66 coincided with reduced standing water, particularly at a depth of 8 cm for Cd and 2 cm for As, underscoring the importance of water management in regulating different metal(loid) mobility. Beyond redox regulation, BF and NBF also modified porewater chemistry by increasing soil pH and moderating E_h (Figure S5, Table S1). In addition, BF and NBF introduced O-containing functional groups (–OH, –COO–) and mineral components capable of complexing or precipitating Cd and As (Fig. 1b) (Tan et al. 2024). Nano-biochar enhanced these adsorption processes by offering higher specific surface area and more reactive sites. Importantly, microbial processes (Sect. 3.2.2) also contributed to the observed porewater dynamics. BF and especially NBF reshaped microbial community composition toward taxa associated with organic matter turnover, metal(loid) binding, and stress tolerance (e.g., Acidobacteriota, Chloroflexota, and Proteobacteria). These shifts likely enhanced microbial-mediated immobilization and transformation of Cd and As, while biochar-derived organic carbon stimulated microbial activity and root exudation of low-molecular-weight organic acids (Jin et al. 2024). Such exudates can transiently mobilize Cd via complexation or influence As speciation through ligand exchange and micro-redox processes, helping to explain the stage-specific peaks observed around heading.

Although the overall temporal trend was similar at 2 cm and 8 cm for both Cd and As, fluctuations were more pronounced near the surface, indicating strong rhizosphere-mediated regulation. Under NPK-I, Cd in porewater did not differ among F, BF and NBF across stages. Under NPK-II, NBF-II tended to maintain lower porewater Cd than BF-II and F-II from heading to maturity ($p<0.05$) (Fig. 4a). Under the NPK-III, NBF-III showed relatively higher Cd in porewater during early vegetative stage ($p<0.05$), but by maturity, both BF-III and NBF-III had lower Cd in porewater than F-III ($p<0.05$), indicating more effective control of Cd specifically at the critical maturation stage. For As, treatment responses were more complex. At NPK-II, F-II generally showed higher As during early growth before booting than BF-II and NBF-II, whereas differences after heading were smaller and sometimes reversed ($p<0.05$) (Fig. 4b). Under NPK-III, NBF-III and BF-III reduced As relative to F-III at germination and seedling, but NBF-III exhibited the largest As peak at heading; by maturity, As concentrations converged to low values across all three treatments, with F-III slightly lower in some cases.

Across all treatments, the concentrations of Cd and As in rice followed the order: root > husk > grain (Fig. 5), indicating restricted translocation to edible grains (Lv et al. 2021). However, their accumulation was significantly influenced by the N:P:K ratio and biochar type. For Cd, BF and NBF generally lowered tissue concentrations compared to the F treatment under NPK-II and NPK-III ($p<0.05$) (Fig. 5a, c, e). Within BF treatments, Cd content was lowest at the NPK-I ratio ($p<0.05$), while in NBF treatments, Cd content in grains tended to be lowest at NPK-III (Fig. 5a), although this difference was not statistically significant. In contrast, the optimal suppression of As occurred under F-II, followed by NBF-I (Fig. 5b, d, f). Overall, Cd inhibition was strongest under F-I and then NBF-III, whereas As control was maximized under F-II and then NBF-I. This discrepancy likely arises from differences in the environmental chemistry and bioavailability of Cd and As (Quintela et al. 2020), coupled with their distinct, plant-mediated uptake and translocation mechanisms (Qin et al. 2023).

Overall, BF and particularly NBF afforded dynamic control of Cd and As mobility across the life cycle, with their benefits most evident during the maturation stage when grain contamination risk is highest. Optimizing the combination of biochar type and N:P:K ratio to minimize porewater Cd and As during heading–maturity is therefore essential for effective remediation and ensuring rice grain safety.

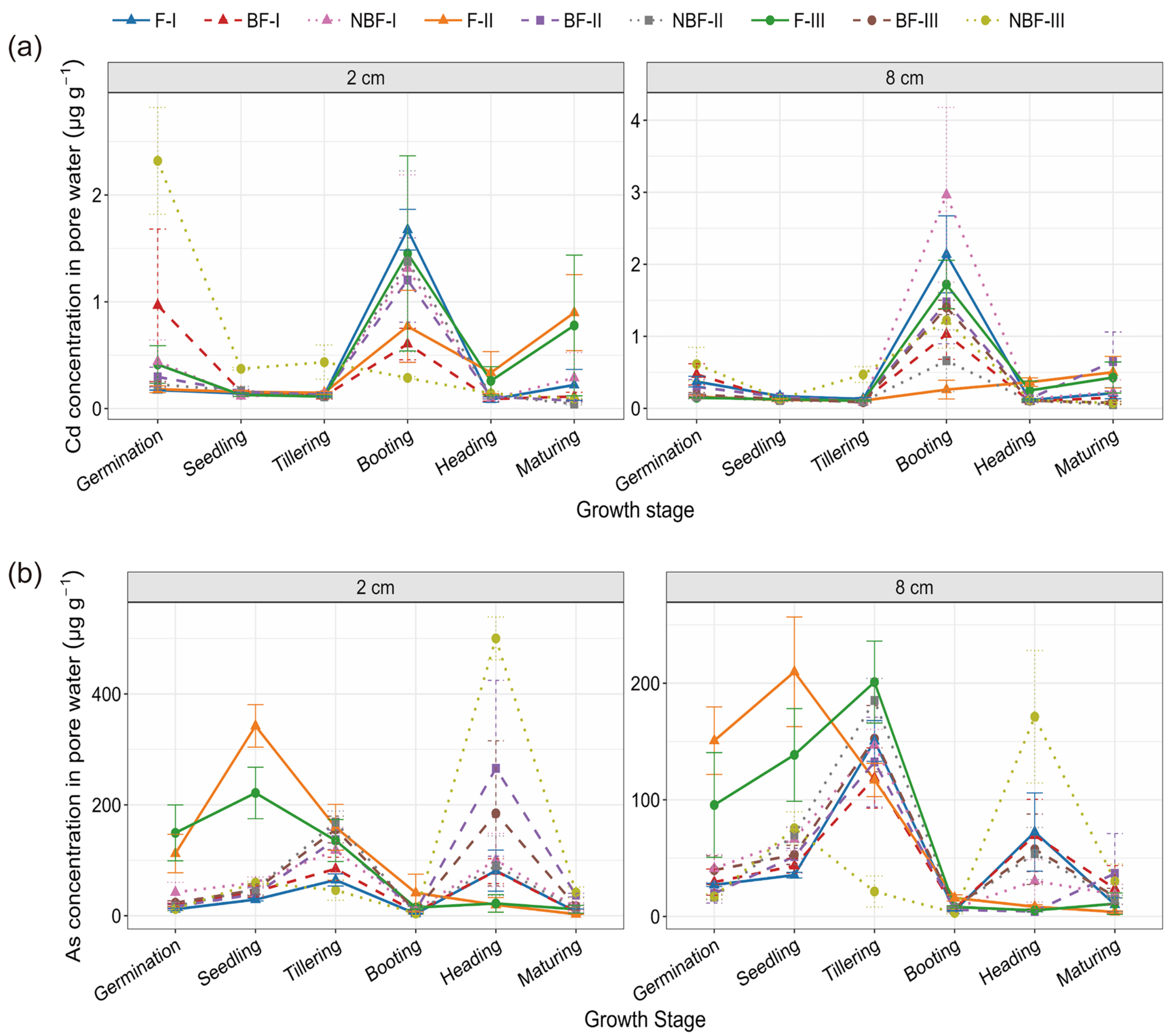

Fig. 4 Temporal variation of **a** Cd and **b** As concentrations in soil porewater during rice cultivation under different fertilizer treatments at 2 and 8 cm depths. Data are reported as the mean ± SE (N = 3)

4 Conclusion

This study systematically evaluated biochar-based fertilizers for remediating Cd and As contamination in rice using a full life-cycle greenhouse study. The results demonstrate that both biochar type (conventional vs. nano-sized) and fertilizer N:P:K ratio significantly regulate rice growth (particularly tillering and heading), and Cd and As accumulation. A crucial interaction between biochar type and NPK ratio indicates that biochar performance cannot be evaluated independently of nutrient formulation. Instead, remediation efficiency depends on a contaminant-specific, nutrient-managed strategy, because the optimal biochar-N:P:K ratio combinations differed for Cd versus As, consistent with their contrasting biogeochemical behaviors in soil–plant systems. Acceleration of tillering and heading under optimized BF and NBF treatments provides agronomic benefits by promoting early canopy establishment, improving nutrient uptake efficiency, and enhancing competitive ability against weeds. Earlier heading may also shorten the duration of vegetative exposure to elevated porewater metal(loid) availability, potentially reducing cumulative uptake before grain filling. The suppression of Cd and As in porewater from heading to maturity is especially relevant for food safety because grain filling and final

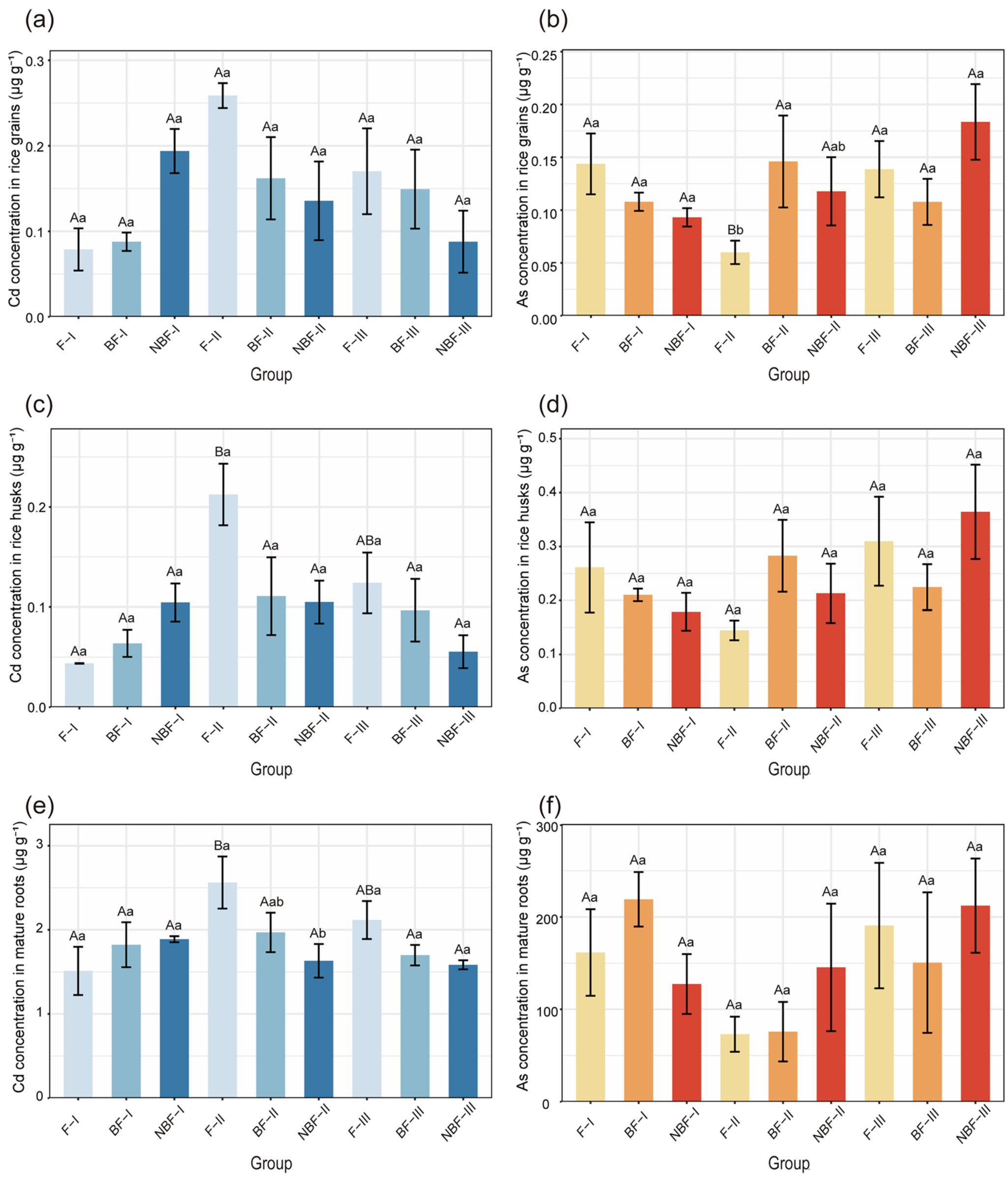

Fig. 5 Cd and As contents in different rice tissues: **a** Cd in grains, **b** As in grains, **c** Cd in husks, **d** As in husks, **e** Cd in roots, **f** As in roots. Uppercase letters indicate significant differences across N:P:K ratios within the same fertilizer treatment ($p < 0.05$). Lowercase letters indicate significant differences among different fertilizers with the same N:P:K ratio ($p < 0.05$). Data are reported as the mean ± SE (N = 5)

Cd and As accumulation in rice grain occur primarily during this period. Importantly, this study identifies that the most effective combination for Cd suppression was nano-biochar with NPK-III, while nano-biochar with NPK-I was optimal for As control. These results refine the conventional 'one-size-fits-all' remediation approach and highlight the value of precision amendment design that jointly considers the dominant contaminant and the accompanying amendment technology. From a practical perspective, the proposed framework supports the development of biochar-based fertilization protocols that can simultaneously improve nutrient management and food-safety risks in contaminated rice-growing regions, which is directly relevant to farmers already applying biochar-based products. However, due to greenhouse space constraints, the study prioritized the detection of large effects. Accordingly, non-significant responses, particularly for small-to-medium effects, should be interpreted with caution.

Future research should focus on field-scale validation of these optimized combinations and their long-term impacts on soil health, contaminant mobility, and rice productivity.

Supplementary Information

The online version contains supplementary material available at https://doi.org/10.1007/s42773-026-00571-6.

Additional file1 (DOCX 3368 kb)

Acknowledgements
The authors thank Chengjia Zhang of the Core Facilities for Life and Environmental Sciences, State Key Laboratory of Microbial Technology (SKLMT) of Shandong University for his help in analyzing metals with ICP-MS. Thanks to Sen Wang, Haiyan Yu, Xiaomin Zhao and Yuyu Guo from SKLMT for the assistance in scanning electron microscopy/focused ion beam microscopy imaging.

Author contributions
Xingyu Yan: Methodology, Formal analysis, Investigation, Writing-original draft. Wenhui Li, Jiawei Wang, Zhongxiang Cao: Formal analysis, Investigation. Jing Liu: Supervision, Methodology, Formal analysis, Investigation, Writing-review & editing, Funding acquisition. Weiying Feng and Jining Li: Funding acquisition, Writing-review. John P Giesy and George P Cobb: Writing-review. All authors read and approved the final manuscript.

Funding
This work was supported by the National Natural Science Foundation of China (42207325), the Environmental Research Institute Young Scholar Future Plan from Shandong University to Jing Liu, the Key Research and Development and Technology Transfer Program of Inner Mongolia Autonomous Region in China (2025YFHH0145), and the Guangdong Foundation for Program of Science and Technology Research (2023B1212060044), and the GDAS' Project of Science and Technology Development (2022GDASZH-2022010104-2).

Data availability
Data is provided within the manuscript or supplementary information files.

Declarations

Competing interests
The authors declare no competing financial interest.

Author details
[1]Environment Research Institute, Shandong University, Qingdao 266237, China. [2]School of Materials Science and Engineering, Beihang University, Beijing 100191, China. [3]School of Environmental Science and Engineering, Shandong University, Qingdao 266237, China. [4]National-Regional Joint Engineering Research Center for Soil Pollution Control and Remediation in South China, Guangdong Key Laboratory of Integrated Agro-Environmental Pollution Control and Management, Institute of Eco-Environmental and Soil Sciences, Guangdong Academy of Sciences, Guangzhou 510650, Guangdong, China. [5]Department of Environmental Science, Baylor University, Waco, TX 76798-7266, USA. [6]Department of Biomedical Veterinary Sciences and Toxicology Centre, University of Saskatchewan, Saskatoon, SK S7N 5B3, Canada. [7]Department of Integrative Biology and Center for Integrative Toxicology, Michigan State University, East Lansing, MI 48824, USA.

Received: 10 December 2025 Revised: 23 December 2025 Accepted: 4 January 2026
Published: 15 February 2026

References

Bolan N, Sarmah A, Bordoloi S et al (2023) Soil acidification and the liming potential of biochar. Environ Pollut 317:120632. https://doi.org/10.1016/j.envpol.2022.120632
Cao X, Liu J, Zhang L et al (2024) Response of soil microbial ecological functions and biological characteristics to organic fertilizer combined with biochar in dry direct-seeded paddy fields. Sci Total Environ 948:174844. https://doi.org/10.1016/j.scitotenv.2024.174844
Chausali N, Saxena J, Prasad R (2021) Nanobiochar and biochar based nanocomposites: advances and applications. J Agric Food Res 5:100191. https://doi.org/10.1016/j.jafr.2021.100191
Chen S, Yang M, Ba C et al (2018) Preparation and characterization of slow-release fertilizer encapsulated by biochar-based waterborne copolymers. Sci Total Environ 615:431–437. https://doi.org/10.1016/j.scitotenv.2017.09.209
Chen S, Tang X, Chen J et al (2025) Regulation of slow-release performance of high-sugar biomass waste filter mud and sugarcane bagasse by co-hydrothermal carbonization and potential evaluation of hydrochar-based slow-release fertilizers. Biomass Bioenerg 193:107557. https://doi.org/10.1016/j.biombioe.2024.107557
Cheng J, Liao Z, Hu SC et al (2022) Synthesis of an environmentally friendly binding material using pyrolysis by-products and modified starch binder for slow-release fertilizers. Sci Total Environ 819:153146. https://doi.org/10.1016/j.scitotenv.2022.153146
Cui Z, Zhang H, Chen X et al (2018) Pursuing sustainable productivity with millions of smallholder farmers. Nature 555:363–366. https://doi.org/10.1038/nature25785
Das KP, Satapathy BK (2024) Highly porous agro-augmenting urea-biochar/polylactic acid-based microfibrous electrospun mats as sustainable controlled release fertilizer carriers. ACS Appl Polym Mater 6:6262–6277. https://doi.org/10.1021/acsapm.4c00386
Dong D, Wang C, Van Zwieten L et al (2019) An effective biochar-based slow-release fertilizer for reducing nitrogen loss in paddy fields. J Soils Sediments 20:3027–3040. https://doi.org/10.1007/s11368-019-02401-8
U.S. Environmental Protection Agency (1996) EPA method 3050B: acid digestion of sediments, sludges, and soils. Available via DIALOG. https://www.epa.gov/esam/epa-method-3050b-acid-digestion-sediments-sludges-and-soils
Faloye OT, Ajayi AE, Alatise MO et al (2020) Nutrient uptake, maximum yield production, and economic return of maize under deficit irrigation with biochar and inorganic fertiliser amendments. Biochar 1:375–388. https://doi.org/10.1007/s42773-019-00032-3
Gai X, Xing W, Cheng W et al (2024) Regulatory mechanism of bamboo biochar dosage on cadmium accumulation in *Salix psammophila*: insights from rhizosphere microbial communities, assembly processes, and interactions. Carbon Res 3:72. https://doi.org/10.1007/s44246-024-00163-8
Gu W, Zhang W, Xiu L et al (2023) Soil aggregate variation in two contrasting rice straw recycling systems for paddy soil amendment over two years. Arch Agron Soil Sci 69:3044–3059. https://doi.org/10.1080/03650340.2023.2196618
Hao H, Shan Y, Li P et al (2025) Heuristic topological graph convolutional network for risk prediction of potentially toxic elements in cultivated soils. Environ Sci Technol 59:16685–16696. https://doi.org/10.1021/acs.est.5c06872
He Q, Li X, Ren Y (2022) Analysis of the simultaneous adsorption mechanism of ammonium and phosphate on magnesium-modified biochar and the slow release effect of fertiliser. Biochar 4:25. https://doi.org/10.1007/s42773-022-00150-5
Jeffery S, Verheijen FGA, van der Velde M et al (2011) A quantitative review of the effects of biochar application to soils on crop productivity using meta-analysis. Agric Ecosyst Environ 144:175–187. https://doi.org/10.1016/j.agee.2011.08.015
Ji H, Abdalkarim SYH, Shen Y et al (2024) Facile synthesis, release mechanism, and life cycle assessment of amine-modified lignin for bifunctional slow-release fertilizer. Int J Biol Macromol 278:134618. https://doi.org/10.1016/j.ijbiomac.2024.134618
Jin F, Piao J, Miao S et al (2024) Long-term effects of biochar one-off application on soil physicochemical properties, salt concentration, nutrient

availability, enzyme activity, and rice yield of highly saline-alkali paddy soils: based on a 6-year field experiment. Biochar 6:40. https://doi.org/10.1007/s42773-024-00332-3
Laird DA, Novak JM, Collins HP et al (2017) Multi-year and multi-location soil quality and crop biomass yield responses to hardwood fast pyrolysis biochar. Geoderma 289:46–53. https://doi.org/10.1016/j.geoderma.2016.11.025
Li C, Ji Y, Li E (2022) Understanding the influences of rice starch fine structure and protein content on cooked rice texture. Starch Starke 74:2100253. https://doi.org/10.1002/star.202100253
Li C, Ji Y, Li E et al (2023) Interactions between leached amylose and protein affect the stickiness of cooked white rice. Food Hydrocolloids 135:108215. https://doi.org/10.1016/j.foodhyd.2022.108215
Li P, Yan M, Li M et al (2024) Migration rules and mechanisms of nano-biochar in soil columns under various transport conditions. Nanomaterials 14:1035. https://doi.org/10.3390/nano14121035
Liang F, Li GT, Lin QM et al (2014) Crop yield and soil properties in the first 3 years after biochar application to a calcareous soil. J Integr Agric 13:525–532. https://doi.org/10.1016/s2095-3119(13)60708-x
Liu J, Wolfe K, Potter PM et al (2019) Distribution and speciation of copper and arsenic in rice plants (*Oryza sativa* japonica 'Koshihikari') treated with copper oxide nanoparticles and arsenic during a life cycle. Environ Sci Technol 53:4988–4996. https://doi.org/10.1021/acs.est.9b00234
Liu Q, Tao Y, Cheng S et al (2020a) Relating amylose and protein contents to eating quality in 105 varieties of Japonica rice. Cereal Chem 97:1303–1312. https://doi.org/10.1002/cche.10358
Liu Q, Wu C, Wei L et al (2024) Microbial mechanisms of organic matter mineralization induced by straw in biochar-amended paddy soil. Biochar 6:18. https://doi.org/10.1007/s42773-024-00312-7
Liu Y, Gao C, Wang Y et al (2020b) Vermiculite modification increases carbon retention and stability of rice straw biochar at different carbonization temperatures. J Clean Prod 254:120111. https://doi.org/10.1016/j.jclepro.2020.120111
Liu Z, Yuan X, Zhang Z et al (2025) Revisiting potassium-induced impacts on crop production and soil fertility based on thirty-three Chinese long-term experiments. Field Crops Res 322:109732. https://doi.org/10.1016/j.fcr.2024.109732
López JE, Saldarriaga JF, Tamayo A (2025) Effect of biogas slurry-modified biochar on Cd immobilization, uptake, translocation, and the bioavailability of N, P, and K in soil. J Soil Sci Plant Nutr 25:6281–6293. https://doi.org/10.1007/s42729-025-02530-9
Lu J, Li Y, Cai Y et al (2023) Co-incorporation of hydrotalcite and starch into biochar-based fertilizers for the synthesis of slow-release fertilizers with improved water retention. Biochar 5:44. https://doi.org/10.1007/s42773-023-00242-w
Lv G, Yang T, Chen Y et al (2021) Biochar-based fertilizer enhanced Cd immobilization and soil quality in soil-rice system. Ecol Eng 171:106396. https://doi.org/10.1016/j.ecoleng.2021.106396
Nayak P, Nandipamu TMK, Chaturvedi S et al (2024) Synthesis, properties, and mechanistic release-kinetics modeling of biochar-based slow-release nitrogen fertilizers and their field efficacy. J Soil Sci Plant Nutr 24:7460–7479. https://doi.org/10.1007/s42729-024-02052-w
Qin Y, Li Z, Sun J et al (2023) Manganese (II) sulfate affects the formation of iron-manganese oxides in soil and the uptake of cadmium and arsenic by rice. Ecotoxicol Environ Saf 263:115360. https://doi.org/10.1016/j.ecoenv.2023.115360
Quintela F, Pino S, Silva F et al (2020) Arsenic, lead and cadmium concentrations in caudal crests of the yacare caiman (Caiman yacare) from Brazilian Pantanal. Sci Total Environ 707:135479. https://doi.org/10.1016/j.scitotenv.2019.135479
Raza A, Li Y, Prakash CS et al (2025) Panomics to manage combined abiotic stresses in plants. Trends Plant Sci 30:1079–1084. https://doi.org/10.1016/j.tplants.2025.03.001
Sani MNH, Amin M, Siddique AB et al (2023) Waste-derived nanobiochar: a new avenue towards sustainable agriculture, environment, and circular bioeconomy. Sci Total Environ 905:166881. https://doi.org/10.1016/j.scitotenv.2023.166881
Shahzadi J, Zaib un N, Ali N, et al (2025) Foliar application of nano biochar solution elevates tomato productivity by counteracting the effect of salt stress insights into morphological physiological and biochemical indices. Sci Rep 15:3205. https://doi.org/10.1038/s41598-025-87399-5
Shi W, Ju Y, Bian R et al (2020) Biochar bound urea boosts plant growth and reduces nitrogen leaching. Sci Total Environ 701:134424. https://doi.org/10.1016/j.scitotenv.2019.134424
Si L, Xie Y, Ma Q et al (2018) The short-term effects of rice straw biochar, nitrogen and phosphorus fertilizer on rice yield and soil properties in a cold waterlogged paddy field. Sustainability 10:537. https://doi.org/10.3390/su10020537
Srivastav AL, Patel N, Rani L, Kumar P et al (2023) Sustainable options for fertilizer management in agriculture to prevent water contamination: a review. Environ Dev Sustain 26:8303–8327. https://doi.org/10.1007/s10668-023-03117-z
Tan T, Xu Y, Liao X et al (2024) Formulating new types of rice husk biochar-based fertilizers for the simultaneous slow-release of nutrients and immobilization of cadmium. GCB Bioenergy 16:e13142. https://doi.org/10.1111/gcbb.13142
Tao K, Yu W, Prakash S et al (2019) High-amylose rice: starch molecular structural features controlling cooked rice texture and preference. Carbohydr Polym 219:251–260. https://doi.org/10.1016/j.carbpol.2019.05.031
Tao Y, Feng W, He Z et al (2024) Utilization of cotton byproduct-derived biochar: a review on soil remediation and carbon sequestration. Environ Sci Eur 36:79. https://doi.org/10.1186/s12302-024-00908-7
Villada E, Velasquez M, Gómez AM et al (2024) Combining anaerobic digestion slurry and different biochars to develop a biochar-based slow-release NPK fertilizer. Sci Total Environ 927:171982. https://doi.org/10.1016/j.scitotenv.2024.171982
Wang L, Wang J, Wang Z et al (2018) Enhanced antimonate (Sb(V)) removal from aqueous solution by La-doped magnetic biochars. Chem Eng J 354:623–632. https://doi.org/10.1016/j.cej.2018.08.074
Wang C, Luo D, Zhang X et al (2022) Biochar-based slow-release of fertilizers for sustainable agriculture: a mini review. Environ Sci Ecotechnol 10:100167. https://doi.org/10.1016/j.ese.2022.100167
Wang J, Sun L, Sun Y et al (2025) Long-term biochar-based fertilizer substitution promotes carbon, nitrogen, and phosphorus acquisition enzymes in dryland soils by affecting soil properties and regulating bacterial community. Appl Soil Ecol 206:105801. https://doi.org/10.1016/j.apsoil.2024.105801
Wu Y, Xi X, Tang X et al (2018) Policy distortions, farm size, and the overuse of agricultural chemicals in China. Proc Natl Acad Sci USA 115:7010–7015. https://doi.org/10.1073/pnas.1806645115
Xiang A, Gao Z, Zhang K et al (2021) Study on the Cd (II) adsorption of biochar based carbon fertilizer. Ind Crops Prod 174:114213. https://doi.org/10.1016/j.indcrop.2021.114213
Xu M, Luo F, Tu F et al (2022) Effects of stabilizing materials on soil Cd bioavailability, uptake, transport, and rice growth. Front Environ Sci 10:1035960. https://doi.org/10.3389/fenvs.2022.1035960
Xue J, Verstraete W, Ni B-J et al (2025) Rethink biosolids: risks and opportunities in the circular economy. Chem Eng J 510:161749. https://doi.org/10.1016/j.cej.2025.161749
Yan S, Ren T, Wan Mahari WA et al (2022) Soil carbon supplementation: improvement of root-surrounding soil bacterial communities, sugar and starch content in tobacco (N. tabacum). Sci Total Environ 802:149835. https://doi.org/10.1016/j.scitotenv.2021.149835
Yang J, Yang F, Yang Y et al (2016) A proposal of "core enzyme" bioindicator in long-term Pb-Zn ore pollution areas based on topsoil property analysis. Environ Pollut 213:760–769. https://doi.org/10.1016/j.envpol.2016.03.030
Yuan Y, Liang Y, Cai H et al (2025) Soil organic carbon accumulation mechanisms in soil amended with straw and biochar: entombing effect or biochemical protection? Biochar 7:33. https://doi.org/10.1007/s42773-025-00431-9
Zhang L, He Y, Lin D et al (2022) Co-application of biochar and nitrogen fertilizer promotes rice performance, decreases cadmium availability, and shapes rhizosphere bacterial community in paddy soil. Environ Pollut 308:119624. https://doi.org/10.1016/j.envpol.2022.119624

Zhang K, Khan Z, Khan MN et al (2024) The application of biochar improves the nutrient supply efficiency of organic fertilizer, sustains soil quality and promotes sustainable crop production. Food Energy Secur 13:e520. https://doi.org/10.1002/fes3.520

Zhao C, Xu J, Bi H et al (2023) A slow-release fertilizer of urea prepared via biochar-coating with nano-SiO2-starch-polyvinyl alcohol: formulation and release simulation. Environ Technol Innov 32:103264. https://doi.org/10.1016/j.eti.2023.103264

Zulfiqar U, Khokhar A, Maqsood MF et al (2024) Genetic biofortification: advancing crop nutrition to tackle hidden hunger. Funct Integr Genomics 24:34. https://doi.org/10.1007/s10142-024-01308-z